

High Precision Energy Measurements from the Analysis of Wide Spectral Features. Application to the fluorescence of YAG:Ce³⁺

Miguel Lagos,^{*} Rodrigo Paredes,[†] and César Retamal[‡]

Facultad de Ingeniería, Universidad de Talca, Campus Los Niches, Camino a los Niches km 1, Curicó, Chile

(Dated: April 12, 2017)

Advantage is taken of a complete and precise experimental study of the luminescent properties of yttrium aluminium garnet doped with Ce³⁺, previously accomplished by other authors, to confirm the accuracy of the invoked theoretical methods for dealing with the realistic calculation of the electromagnetic spectra of condensed phases. The fluorescent spectra at $T = 0$ and $T = 250$ K of YAG:Ce³⁺ were calculated with no adjustable parameter, giving complete agreement with experiment. The energy released by the electronic transitions was determined with precision better than 5% the full width at half maximum of the spectral features. Thermal quenching of the fluorescent yield is discussed and calculated in a less accurate way, but anyway showing good agreement with experiment.

PACS numbers: 33.70.-w, 33.50.-j, 78.20.Bh

Fluorescence is generally associated to transitions of a local electronic orbital causing a significant structural variation, and hence a strong perturbation of the dynamics of nuclear degrees of freedom. The absent, or very weak [1], zero-phonon line in the observed spectra proves in empirical way that few-phonon processes are infrequent. The wide frequency spectra of the exchanged photons, the large Stokes shifts and peak asymmetries, and the marked dependence of the spectral features on the local and long-range properties of the hosting medium, have all them a common explanation: the large amount of energy spent in exciting acoustic traveling waves in the medium hosting the fluorescent molecule [2, 3]. From a thermodynamic standpoint, the electronic and electromagnetic radiation fields are two weakly coupled systems going through a transformation between two well defined states, in thermal equilibrium with the energy reservoir constituted by the acoustic vibrational modes of the extended material medium. By the entropy law, the thermal bath always takes a positive amount of energy in the average. In photon absorption processes the radiation field statistically provides the energy delivered to the thermal bath, and the electron field does in the emission events. Then the Stokes shift is a direct consequence of the second law of thermodynamics. Peak asymmetries have a similar general explanation, since photons carrying an energy excess, or defect, are more probable in absorption, or emission, processes.

The technology of fluorescence has advanced at an accelerating pace in a variety of applications [4–6]. Many of them follow from the sensitivity of the optical properties of the fluorophores to the physical attributes of the embedding medium [7–13]. Despite these advances, there are still some aspects which deserve deeper under-

standing. Recent papers report a theoretical framework able to reproduce with high numerical precision the temperature dependent lineshapes [2] and quenching [3] of the fluorescent spectra of molecules in a condensed environment. The purpose of this communication is to take advantage of a thorough and complete study of the optical properties of YAG, previously published by other authors [1], to briefly show the power of the methods for the analysis of fluorescent spectra put forward in these papers [2, 3], and the convenience of having at hand a good theoretical tool for analyzing the empirical facts.

Yttrium aluminum garnet (Y₃Al₅O₁₂ or YAG) doped with Ce³⁺ is a phosphor widely applied in white LEDs for converting blue to yellow light, among many other technical applications. Fed by the violet and blue lines of the commonly employed halophosphate phosphor, YAG:Ce³⁺ produces a broad emission band shifted to yellow which combines with the white light of the LED phosphor to make it warmer. The experimental study of Bachmann et al. is particularly useful because exhibits spectra taken at temperatures from near $T = 0$ up to $T = 600$ K [1]. However, what makes this experiment special is that the resolution was large enough to clearly observe at 489 nm the zero-phonon line of one of the two partially superimposed emission bands. This quite unusual observation in fluorescent spectra gives not only the absolute energy released in the main electronic transition, $^2d \rightarrow ^2F_{5/2}$, as $E = 2.535$ eV [1, 14], but also the probability of a zero-phonon event. A shoulder in the spectral maximum suggests the contribution of a competing secondary transition, interpreted as $^2d \rightarrow ^2F_{7/2}$ [1, 14]. The relative intensity of the zero-phonon line at a temperature $T = 4$ K is 0.27% of the total intensity of the main emission band.

In general, the lineshape function is given by the function [2, 3, 15, 16]

^{*}Electronic address: mlagos@utalca.cl

[†]Electronic address: raparede@utalca.cl

[‡]Electronic address: ceretamal@utalca.cl

$$F(\hbar ck; T) = \frac{a}{\pi \hbar v_s} \int_{-\infty}^{\infty} d\tau \exp \left\{ -\alpha [J(\tau; T) - J(\infty; T)] \right\} \\ \times \exp \left\{ i \left[\alpha I(\tau) - \frac{2a}{\hbar v_s} (\hbar ck - E) \tau \right] \right\} \\ + \exp \left[-\alpha J(\infty; T) \right] \delta(\hbar ck - E), \quad (1)$$

where $\hbar ck$ is the photon energy, E the energy difference of the two electronic states involved in the transition, a is essentially the bond length, and v_s the mean speed of sound of the acoustic modes of vibration of the medium. The general form of the auxiliary functions $J(\tau; T)$ and $I(\tau)$ depends on the symmetry of the surroundings of the optically sensitive orbital [16]. For the simplest case of octahedral symmetry they read

$$J(\tau; T) = \int_0^{aq_D} \frac{dx}{x} \left(1 - \frac{\sin x}{x} \right) \coth(\beta x) \sin^2(\tau x), \quad (2)$$

$$I(\tau) = \frac{1}{2} \int_0^{aq_D} \frac{dx}{x} \left(1 - \frac{\sin x}{x} \right) \sin(2\tau x), \quad (3)$$

with q_D being the cutoff for the wavenumber of acoustic waves, and the adimensional magnitudes appearing in the lineshape function $F(\hbar ck; T)$ are given by [2]

$$\alpha = \frac{3(\Delta F)^2}{\pi^2 \hbar \rho v_s^3} \quad \beta = \frac{\hbar v_s}{2ak_B T} \quad \tau = \frac{v_s}{2a} t, \quad (4)$$

where k_B is the Boltzmann constant, T the temperature, α an electron-phonon coupling constant, and

$$J(\infty; T) = \frac{1}{2} \int_0^{aq_D} \frac{dx}{x} \left(1 - \frac{\sin x}{x} \right) \coth(\beta x). \quad (5)$$

The second term in the right hand side of Eq. (1) for $F(\hbar ck; T)$, containing the delta-function is the zero-phonon line, and the first one the phonon broadened distribution. The lineshape function $F(\hbar ck; T)$ is normalized as [2, 15, 16]

$$\int_{-\infty}^{\infty} d(\hbar ck) F(\hbar ck; T) = 1 \quad (6)$$

and hence the relative contribution of zero-phonon processes to the total fluorescent yield is

$$I_{ZPL} = \exp \left[-\alpha J(\infty; T) \right]. \quad (7)$$

Bauchmann et al. measured $I_{ZPL} = 0.0027$ at $T = 4$ K. At $T \approx 0$, Eq. (5) does not depend on the constant β because the hyperbolic function goes rapidly to unity as β

grows. With practically no precision loss, one can replace $J(\infty; 4 \text{ K})$ by $J(\infty; 0 \text{ K}) = 0.5817$. This way, the low temperature data allows to determine the constant α

$$0.0027 = \exp(-\alpha \times 0.5817) \implies \alpha = 10.17. \quad (8)$$

It is assumed here that $aq_D = (12\pi^2)^{1/3}$, corresponding to octahedral symmetry.

On the other hand, the maximum of the main peak of the $T = 4$ K spectrum is at $\lambda = 523 \text{ nm}$ (2.370 eV). As the zero phonon line is at $\lambda = 489 \text{ nm}$ (2.535 eV) the contribution to the Stokes shift of emission is the difference 0.165 eV. This result is useful to determine the energy scale factor in Eq. (1) that puts the maximum of the distribution in the right place. This gives

$$\frac{\hbar v_s}{2a} = 8.8121 \times 10^{-22} \text{ J} = 0.00550 \text{ eV}. \quad (9)$$

The mean speed of sound in YAG is $v_s = 5.47 \times 10^3 \text{ m/s}$ [17]. Replacing in Eq. (9), one obtains that $a = 32.7 \text{ nm}$, which is a very reasonable value. The calculated distance of substitutional Ce^{3+} in YAG to the nearest oxygen neighbors is 23–24 nm [18]. The figure for a is closer to the six Al^{3+} neighbors with coordination quasioctahedral, whose distances to the Ce^{3+} ion are 30.0 and 33.6 nm [18]. Hence the assumption of octahedral symmetry for aq_D is consistent with the predominance of the bonding of the Ce^{3+} ions with their Al^{3+} next-neighbors.

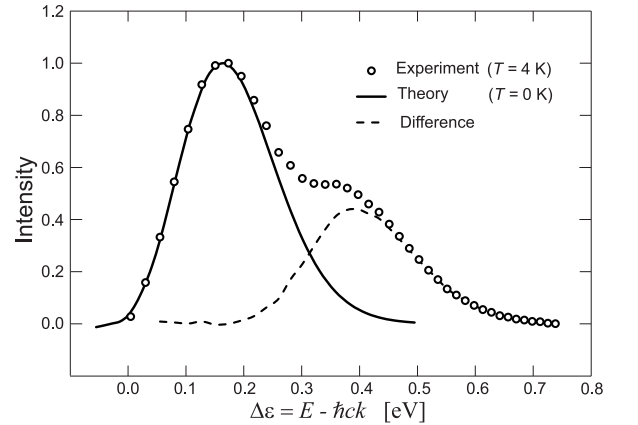


FIG. 1: Open circles represent the fluorescent emission spectrum of YAG: Ce^{3+} at $T = 4$ K, as measured by Bauchmann et al. [1]. The solid line represents Eq. (1) with constants determined from the experiment and no fitting parameter. The origin of $\Delta\epsilon$ is in the energy of the zero-phonon line of the transition ${}^2d \rightarrow {}^2F_{5/2}$. The broken line is the difference, evidencing the existence of a competing transition, presumably ${}^2d \rightarrow {}^2F_{7/2}$.

Knowing the two constants α and $\hbar v_s/(2a)$ the lineshape function (1) can be evaluated for $T = 0$. The resulting curve is shown in Fig. 1, together with the experimental data of Bauchmann et al. for $T = 4$ K. The

coincidence between theory and the main feature of the experimental spectrum (attributed to the $5d^1 \rightarrow {}^2F_{5/2}$ transition [14]) is remarkable, particularly because the theoretical curve has no adjustable parameter.

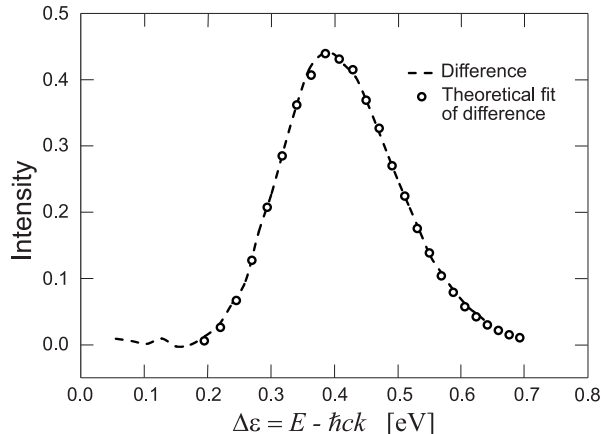


FIG. 2: The broken line depicts the difference between the theoretical curve and experimental data shown in Figure 1. Open circles represent Eq. (1) with the coupling constant α as a fitting parameter and $\Delta\epsilon$ displaced in 0.192 eV in order to describe the second transition ${}^2d \rightarrow {}^2F_{7/2}$.

The broken lines in Figs. 1 and 2 represent the difference between the experimental data and the theoretical curve for $\alpha = 10.17$ and $\hbar v_s/(2a) = 0.00550$ eV. Interpreting this new data set as the emission attributed to the transition $5d^1 \rightarrow {}^2F_{7/2}$ [14], a theoretical fit of it is essayed with the lineshape function (1), with the coupling constant $\alpha = 12.3$, same energy scale constant $\hbar v_s/(2a) = 0.00550$ eV, and the photon energies shifted in 0.192 eV. The new zero phonon line is then at $E' = 2.343$ eV, which is the net energy released in the second transition. As shown by Fig. 2, the correspondence between theory and experiment is again very good. The displacement of the energy transfers affects also the zero-phonon line and the net energy released in the second transition. Table 1 summarizes the situation.

TABLE I: Energy released in the electronic transitions.

Transition	Energy [eV]
${}^2d \rightarrow {}^2F_{5/2}$	2.535
${}^2d \rightarrow {}^2F_{7/2}$	2.343

The empirical data we are comparing with are normalized by setting the maxima of the distributions at unity. The theoretical curve of Fig. 1 was normalized accordingly, dropping the factor preceding the integral in Eq. (1) and multiplying it by a weight factor 12.00 to put the maximum at unity. The fit of the theoretical curve and the data in Fig. 2 was attained by the same

procedure with a weight factor 5.71. Thus the ratio of the intensities of the two emission bands is close to 2:1.

The constants α and $\hbar v_s/(2a)$ are enough to determine the line shape at any temperature through Eq. (1). The integrated intensities, or quantum yields, constitute a different matter because competitive non radiative decay channels may exist, giving rise to temperature dependent quenching of the quantum efficiency. The shape of the absorption and emission bands, given by Eq. (1), are not affected because quenching is in general due to the simultaneous draining of the excited states by an alternate non radiative process [3]. The emission probabilities per unit time of photons of different energies are then affected the same way, and their relative values are not changed.

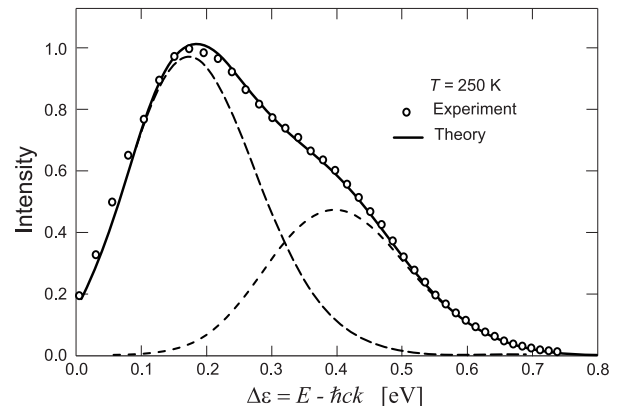


FIG. 3: Emission intensity at $T = 250$ K. Broken lines depict the contribution of the two transitions, as given by Eq. (1) with the same constants determined from the analysis of the $T = 0$ data. Circles represent the data of Bachmann et al. [1]

The calculations for $T = 0$ were repeated for $T = 250$ K, yielding the curves of Fig. 3. They were obtained conserving $\alpha = 10.17$ and 12.3 for the 2.535 eV and 2.343 eV transitions, respectively, and $\hbar v_s/(2a) = 0.0550$ eV. This gives $\beta = 0.2553$ for $T = 250$ K. The broken lines represent the contributions of the two transitions, and the solid line is the sum of both with weighting factors 13.95 and 7.50. Although the ratio of the intensities varied a little with respect to the case $T = 0$, it is still close to 2:1. Actually, the ratio between the intensities of the two contributions differs from 2:1 by 5% and -7% at $T = 0$ and $T = 250$ K, respectively. This suggests that the transition contributing the most may be connected with the four coplanar Al^{3+} next-neighbors to the Ce^{3+} ion, and the remaining two Al^{3+} ions of the quasi-octahedral array be connected with the weaker contribution.

A deep study on the problem of quenching and its temperature dependence has been recently published [3]. The theoretical investigation of the thermal quenching of $\text{YAG}:\text{Ce}^{3+}$ is particularly interesting because has been the subject of thorough experimental study of Bachmann et al. The predicted quantum yield given by Eq. (1) is

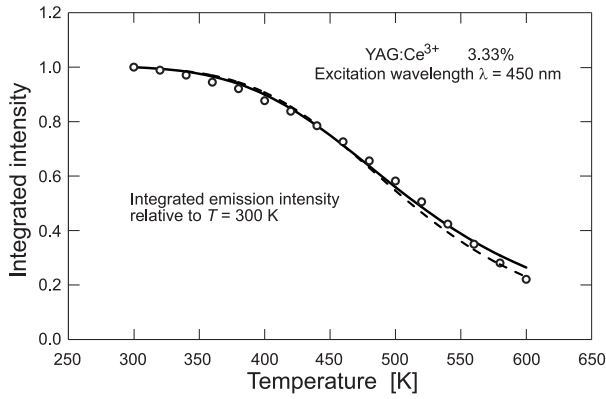


FIG. 4: Temperature dependence of the quantum yield of the fluorescence of 3.33% concentration YAG:Ce³⁺, excited by light of 450 nm wavelength [1]. Circles stand for experiment and the solid line represents the approximate Eq. (10) with $p = 2.20 \times 10^{-7} \text{ J}^{1/2}$ and $\varepsilon = 0.350 \text{ eV}$. The meaning of the broken line is discussed in the text. Experimental and theoretical results show some discrepancies because Eq. (10) is an asymptotic expression valid under conditions which are not fully satisfied here.

always unity, as expressed by Eq. (6), independent of the temperature and particularities of the hosting medium. This is because the derivation of Eq. (1) assumes a single decay channel and drops terms of the system Hamiltonian which becomes significant when the coupling of the electronic and configurational variables become strong enough, as occurs in fluorescent solids or molecules in a condensed medium. These terms do not contain variables of the radiation field and give rise to non radiative decay channels which compete with the radiative contribution [3].

The temperature dependent integrated intensity, or quantum yield, of YAG:Ce³⁺ fluorescence deserves a detailed study. By the time being we will simply apply the asymptotic equation for the ratio of the quantum yield $\phi(T)$ at two temperatures, T and a reference temperature T_0 [3],

$$\frac{\phi(T)}{\phi(T_0)} = \frac{1 + \frac{p}{\sqrt{k_B T_0}} \exp\left(-\frac{\varepsilon}{k_B T_0}\right)}{1 + \frac{p}{\sqrt{k_B T}} \exp\left(-\frac{\varepsilon}{k_B T}\right)}, \quad (10)$$

which holds for high temperatures and strong enough electron-phonon coupling. The latter is made apparent by the breadth of the spectral maximum. Eq. (10) has proven to reproduce with great accuracy the tem-

perature dependent yield efficiency of dissolved 8-methoxypsoralen, which displays a single fluorescent maximum of 0.6 eV full width at half maximum (FWHM) [3]. However, the maxima exhibited by YAG:Ce³⁺ do not go beyond 0.25 eV FWHM, and then the accuracy of the simple Eq. (10) in the present case may be less than perfect. Fig. 4 shows the data of Bauchmann et al. for the ratio expressed in the right hand side of Eq. (10) with $T_0 = 300 \text{ K}$ (circles). The solid line represents Eq. (10) with the constants $p = 2.20 \times 10^{-7} \text{ J}^{1/2}$ and $\varepsilon = 5.61 \times 10^{-20} \text{ J} = 0.350 \text{ eV}$. The fit of the theoretical curve to the experimental data is fairly good for values of the constants which have the expected magnitudes. However small but systematic deviations do exist. Beside the rather insufficient width of the spectral maximum, the temperature range is another source of errors. The mean speed of sound in YAG is $v_s = 5.47 \times 10^3 \text{ m/s}$ [14], which is a rather high value. Hence the Debye temperature is expected to be high as well, higher than 300 K. As the Debye temperature is the reference for temperatures, Eq. (10) is expected to be not very precise in the interval $300 \text{ K} < T < 600 \text{ K}$. The temperature dependent quantum yield curves reported by Bachmann et al. vary with the Ce³⁺ concentration and wavelength of the exciting light. Independence of these variables is attained for just the highest concentration (3.33%). The effect is presumably due to the formation of small clusters of the substitutional Ce impurities. The local distortions they produce in the lattice give rise to an attractive interaction. These hypothetical clusters would be less regular for lower concentrations, giving rise to the dependence on exciting wavelength and concentration. By this reason Fig. 4 takes the data of the higher 3.33% concentration.

The broken line in Fig. 4 represents the curve given by an equation similar to Eq. (10), but with the factor $p/\sqrt{k_B T}$ replaced by the numerical constant 3420 and $\varepsilon = 5.75 \times 10^{-20} \text{ J} = 0.359 \text{ eV}$. This was done because this kind of equation has been essayed in the literature for fitting the temperature dependence of the thermal quenching of luminescence. Also, the broken line in Figure 4 shows that, although multiplying a strongly varying exponential factor, the temperature dependence of the pre-exponential factor is not completely lost and can be elucidated from the analysis of the data.

Acknowledgments. This work was partially supported by the research fund Enlace-Fondecyt, Dirección de Investigación, Universidad de Talca, Chile (M. L. and R. P.), also by CONICYT, FONDECYT, Chile, under Grant No. 1131044, (R. P.). C. R. acknowledges financial support from CONICYT, FONDECYT Iniciación, Chile, under Grant No. 11130624.

[1] V. Bachmann, C. Ronda, A. Meijerink, Chem. Mater. **21**, 2077 (2009)

[2] M. Lagos, R. Paredes, J. Phys. Chem. A **118** 10754, (2014).

- [3] M. Lagos, R. Paredes, *Solid State Communications* **242**, 52 (2016).
- [4] J. R. Lakowicz, **Principles of Fluorescence Spectroscopy**, Springer, New York, 2006.
- [5] S. Mukamel, **Principles of Nonlinear Optical Spectroscopy**, Oxford University Press, New York, 1995.
- [6] **Molecular Probes Handbook** (online version) lifetechnologies.com/handbook.
- [7] A. Marini, A. Muñoz-Losa, A. Biancardi, B. Mennucci, *J. Phys. Chem. B* **114**, 17128, (2010).
- [8] M. A. Haidekker, T. P. Brady, D. Lichlyter, E. A. Theodorakis, *Bioorganic Chem.* **33**, 415 (2005).
- [9] M. L. Horng, J. A. Gardecki, A. Papazyan, M. Maroncelli, *J. Phys. Chem.* **99**, 17311, (1995).
- [10] Z. Diwu, Y. Lu, C. Zhang, D. H. Klaubert, R. P. Haugland, *Photochemistry and Photobiology* **66**, 424 (1997).
- [11] T. Lai, B. T. Lim, E. C. Lim, *J. Am. Chem. Soc.* **104**, 7631 (1982).
- [12] A. Safarzadeh-Amiri, M. Thompson, U. J. Krull, *Journal of Photochemistry and Photobiology, A: Chemistry* **47**, 299 (1989).
- [13] R. B. Macgregor, G. Weber, *Nature* **319**, 70 (1986).
- [14] Z. Yanfang, L. Lan, Z. Xiaosong, X. Qun, *J. Rare Earths* **26**, 446 (2008).
- [15] M. Lagos, F. Asenjo, R. Hauryón, D. Pastén, P. S. Moya, *J. Phys. Chem. A* **114**, 7353 (2010).
- [16] M. Lagos, F. Asenjo, R. Hauryón, D. Pastén, H. González, R. Henríquez, R. Troncoso, *Phys. Rev. B* **77**, 104305 (2008).
- [17] X. Zhan, Z. Li, B. Liu, J. Wang, Y. Zhou, and Z. Hu, *J. Am. Ceram. Soc.* **95**, 1429 (2012).
- [18] J. Gracia, L. Seijo, Z. Barandiarán, D. Curulla, H. Niemansverdriet, W. van Gennip, *J. Lumin.* **128**, 1248 (2008).